Damping Behavior of Entangled Comb Polymers: Experiment

Jung Hun Lee,*,† Paraskevi Driva,‡ Nikos Hadjichristidis,‡ Pamela J. Wright,† Steven P. Rucker,† and David J. Lohse†

ExxonMobil Research and Engineering Company, Annandale, New Jersey 08801, and Department of Chemistry, University of Athens, Panepistimiopolis Zografou, 15771 Athens, Greece

Received October 9, 2008; Revised Manuscript Received December 3, 2008

ABSTRACT: The stress relaxation dynamics of entangled polyisoprene comb polymers were investigated, specifically under nonlinear step deformations, in order to identify the damping mechanism characteristic of comb topology. The damping behavior of two different comb polymers with branches of two and four entanglement lengths clearly exhibited less strain softening (type B) above the universal Doi−Edwards damping function at all strains. However, the corresponding damping functions gradually approached the universal Doi−Edwards damping function with increasing observation time. The observed type B behavior was clearly different from that of H-shaped/multibranch and dendritic star polymers exhibiting a novel damping transition from type B toward the universal Doi−Edwards damping function (i.e., the branch-point withdrawal motion). These results support the proposal that the damping mechanism for combs is due to the gradual stretching and retracting motions caused by branches at the multiple branch points along the comb backbone.

1. Introduction

Molecular theories based on tube confinement have significantly improved the general understanding of the relaxation dynamics of monodisperse entangled linear and branched polymers.[1–8] Moreover, recent advances in anionic synthesis techniques have provided macromolecules with well-defined branches to investigate the effect of specific architectures on the rheological properties.[9–14] For example, the linear viscoelastic properties of model branched polymers with star,[2] H-shaped,[3] multibranch (pom-pom),[4,5] and comb[6–8] architectures can be well predicted, certainly beyond just a qualitative match, using hierarchical tube model theories. On the other hand, fundamental studies of nonlinear properties, especially for model branched architectures,[1,3,5,15–20] are quite rare. Such studies can provide direct insights into the relationships between molecular architectures and nonlinear flow properties. While it is well-known that nonlinear properties of commercial branched polymers like low-density polyethylene (LDPE) are different from those of linear polymers, the basic mechanisms responsible for such differences have not been well understood mainly due to insufficient structural information.

A decade ago, McLeish[15] proposed a theoretical picture of nonlinear behavior under step deformations for H-shaped topology as the branch-point withdrawal motion caused by the stretched chain segments between two branch points. The relaxation modulus $G(\gamma,t)$ after the imposition of step strains is usually expressed in terms of a damping function, $h(\gamma) = G(\gamma,t)/G(t)$, with the equilibrium modulus $G(t)$ as $G(\gamma,t)$ at $\gamma \ll 1$.[1,16] In most cases, the experimental values of $h(\gamma)$ for monodisperse linear polymers with weak or moderate entanglement densities are in good agreement with the universal damping function of the Doi−Edwards tube model theory h_{DE}. On the other hand, branched polymers such as LDPE exhibit a weaker strain dependence (type B) and show values of the damping functions above the universal damping h_{DE}.[16] Such a difference in damping behavior is believed to be due to a retraction process, where the stretched chain segments may not immediately retract to the contour length allowed by the thermal motions of the chain free ends.[3,15–17,19] In the case of H-shaped topology, the inner backbone, trapped between two branch points, becomes stretched according to applied strains. Once the degree of the inner backbone stretching reaches a critical limit, the tension to maintain its contour length becomes large enough to pull the branch point into the confining tube. Then, the branches drawn into the confining tube can no longer hinder the retracting motions of the stretched backbone. This pulling motion, named the branch-point withdrawal, is experimentally observable as a damping transition from type B damping to the universal damping h_{DE}. Recently, Archer et al.[5,16] experimentally confirmed the predicted branch-point withdrawal motion using multibranch polybutadiene polymers. More recently, Lee et al.[20] measured the damping behavior of polyisoprene and polybutadiene second-generation dendritic star polymers and observed similar damping transitions in that topology. All of the above experimental results combined with the theoretical picture suggest that a sudden retraction at large strains is a nonlinear characteristic of branched architectures containing symmetric Y-shaped structural units (e.g., the half of H-shaped/multibranch polymers or the two outer arms with one inner arm in second-generation dendritic star polymers). Therefore, nonlinear measurements on polymers with well-defined branched architectures provide clues to extract the nonlinear characteristics belonging to specific architectures.

From this viewpoint, the damping behavior of comb polymers, especially those with entangled branches, is of interest for investigating the effect of comb topology on the nonlinear relaxation dynamics. An obvious structural feature of comb polymers is their multiple branch points along the linearlike backbone, which are not present in H-shaped/multibranch or dendritic star polymers. The effect of H-shaped topology (equivalent to a comb architecture with only two branches) is well understood, so the incremental effect of having more than two branch points can be characterized via the step strain measurement. If the effect of the comb ends, which look like the Y-shaped structural units, becomes dominant, the damping function should exhibit a sudden retraction at large strains, just like H-shaped/multibranch polymers. On the other hand, type B damping may persist at all strains if the large number of branches at the multiple branch points continue to hinder the retracting motions. Of course, not only the number of branch points but also the size of branches can complicate the nonlinear relaxation dynamics. Recently, Vega and Milner[21] reported the

* Corresponding author. E-mail: menthol88@hotmail.com.
† ExxonMobil Research and Engineering Company.
‡ University of Athens.

10.1021/ma8022662 CCC: $40.75
Published on Web 01/22/2009

Table 1. Molecular Characteristics of Polyisoprene Comb Polymers

polymer	$M_{w,branch}$ [kg/mol]	$M_{w,total}$ [kg/mol]	M_w/M_n (comb)	$\omega_{crossover}$ [rad/s]	$\omega_{\eta''_{max}}$ [rad/s]	q by ^{1}H NMR method I	q by ^{1}H NMR method II	q_{model}
PI Comb14	17.9	241.2	1.04	4.679×10^{-2}	2.512×10^{-2}	5.5	5.1	5
PI Comb15	9.2	127.0	1.01	2.565	1.334	4.4	3.7	4

damping behavior of hydrogenated model polybutadiene comb polymer solutions with linear polyethylene and polyethylene wax. Counterintuitively, more diluted hydrogenated comb solutions exhibit stronger type B damping away from h_{DE}. This trend might be a consequence of dominant diluents repressing the branching effect from the comb architecture and so making relaxation time scales faster than the measurement time scale.

In this article, we focus on the damping behavior of entangled polyisoprene comb polymers in order to identify the damping mechanism of polymers with a comb topology. These comb polymers contain more than three branch points to differentiate them from H-shaped molecules. Also, the size of branches was chosen to be more than two entanglement lengths, enough to exhibit the branching effect. Thus, the linear viscoelasticity was anticipated to exhibit two minima in tan(δ) and/or $G''(\omega)$ as a result of the faster relaxing branches in comb topology. Because the branches are randomly placed along the backbone, these comb polymers had distributions in both branch number and arrangement (the spacing between two adjacent branch points) along the backbone. Although the branches were not precisely spaced along the backbone, the measured linear viscoelasticity did exhibit the relaxation hierarchy of two due to the faster branch relaxation. However, the damping behavior was expected to provide clues to the given comb architecture. That is, if branches were densely placed along one section of the backbone, either at the backbone end or at the middle of the backbone, the damping behavior of such a comb would be expected to be similar to that of star polymers, since the backbone segments trapped between adjacent two branch points become negligible. On the other hand, if polymers with two branches, as opposed to those with more than three branches, dominate the branch number distribution, the corresponding damping behavior should display branch-point withdrawal motion. Thus, the damping behavior should reflect the features of comb topology more sensitively than the linear viscoelasticity.

2. Experiment

2.1. Materials. Well-defined polyisoprene (PI) comb polymers were synthesized by the macromonomer strategy using the 4-(chlorodimethylsilyl)styrene (CDMSS) linkmer (linking agent/monomer) and high-vacuum techniques. Details of the synthesis are provided in recent papers[9–11] and can be summarized in the following steps: (a) anionic polymerization of isoprene to afford living polyisoprene, the branches of the desired combs, (b) selective titration of the chlorosilane group of CDMSS with living polyisoprene to produce the styrenic macromonomer of polyisoprene, and (c) anionic copolymerization of the polyisoprene macromonomer with isoprene, in the presence of a randomizer, to give the final random combs.

Molecular weights of the branches and final products were characterized by size exclusion chromatography with multiangle light scattering (SEC-MALLS). An Agilent Model 1100 solvent pump, autosampler, and degasser form the solvent delivery system for the SEC instrument. The column set consists of three Polymer Laboratories PLgel 10 μm Mixed-B LS columns (300 × 7.5 mm), housed in a column compartment at ambient temperature. Data were acquired with a DAWN multiangle light scattering detector, a ViscoSTAR viscometer, and an OptiLab rEX differential refractive index detector (all detectors from Wyatt Technology Corp.) The detectors were maintained at ambient temperature or, if equipped with temperature control, 25 °C. The instrument was operated at a flow rate of 1.0 mL/min tetrahydrofuran (THF) (EMD Chemicals), inhibited, and prefiltered to 0.2 μm with a typical sample injection volume of 100 μL. All samples were dissolved in THF and prefiltered (0.22 μm) before injection. Molecular weights were determined using Wyatt Technology ASTRA 5 software.

The final products were also analyzed with ^{1}H NMR in order to determine how many silylstyrene linking groups were incorporated per comb. Since each styrenic linker represents a polyisoprene (PI) branch, this should also give a count of the number of branches. We found no evidence of unincorporated styrenic macromonomer. The proton spectra were acquired with a 5 mm autotune probe on a JEOL ECX-400 spectrometer. The samples were prepared in 1,1,2,2-tetrachloroethane-d_2, without Cr(acac)$_3$ relaxation agent. The spectra were acquired with a 9.1 s total repetition time. Free induction decays of 2000 coadded transients were acquired at a temperature of 30 °C.

We determined the silylstyrene content in two ways. In method I, we integrated the aromatic and the silylmethyl regions and divided the integrals by four and six, respectively, to correct for the proton count in each. In method II, we used only the silylmethyl integral, since the probe exhibits a slight aromatic background signal. The isoprene content was determined by adding the olefinic and aliphatic integrals and dividing by eight to account for the eight protons per isoprene. The ratio of isoprene count to silane count gives the number of isoprene units per linker group. This can be converted to the weight of isoprene per linker by multiplying by the formula weight of isoprene (68.12 g/mol). In order to cast this value as branches per chain, we need to divide the measured M_n of the comb by the "M_n per linking group" calculated above. This result gives the number of branches per comb, which is tabulated in Table 1. On the basis of the results of only two samples, we are unable to determine the relative accuracy of the two methods. Since the results of the two methods were not far apart, we have used an average of them in the model calculations described below.

2.2. Rheological Measurements. Stress relaxation dynamics were quantified using small-amplitude oscillatory shear measurements. A Rheometrics Scientific Inc. (RSI) ARES-LS rheometer with 10 mm diameter parallel-plate fixtures was used for all experiments in linear regime. Dynamic storage and loss moduli, $G'(\omega)$ and $G''(\omega)$, of combs were measured at temperatures ranging from −40 to 28 °C. Orchestrator software was used to generate master curves at a reference temperature T_{ref} = 28 °C by a two-dimensional residual minimization method (e.g., allowing horizontal and vertical shifting with residual minimization algorithms). The WLF fit for the shift a_T, $\log(a_T) = [-C_1(T - T_{ref})]/[C_2 + T - T_{ref}]$, yields $C_1 = 5.3 \pm 0.4$ and $C_2 = 146 \pm 8$ °C. These values are similar to $C_1 = 5.1 \pm 0.5$ and $C_2 = 143 \pm 7$ for second-generation polyisoprene dendritic star polymers[20] or $C_1 = 5.0$ and $C_2 = 140$ for polyisoprene asymmetric star polymers[22] but larger than those of $C_1 = 4.1$ and $C_2 = 122$ for linear polyisoprene[23] or $C_1 = 4.5 \pm 0.3$ and $C_2 = 136 \pm 6$ for linear polyisoprene.[24]

The nonlinear relaxation modulus $G(\gamma,t)$ was measured after the imposition of step strains using an Anton Paar Physica modular compact rheometer (MCR501) with 10 mm diameter cone-and-plate (angle = 2°) fixture at 28 °C. In order to ensure complete relaxation between sequential step shear experiments, each measurement was made over a period more than 100 times longer than the evaluated terminal relaxation time $\tau_{\eta''} = 1/\omega_{\eta''}$. This time is the reciprocal of the frequency $\omega_{\eta''}$ at which $\eta''(\omega) \equiv G'(\omega)/\omega$ manifests a local maximum. For example, one measurement after imposition of a step deformation took 6010 s for PI Comb14, for which $\tau_{\eta''}$ was 39.8 s. The damping function $h(\gamma) = G(\gamma,t)/G(t)$ was quantified using the relaxation modulus $G(\gamma,t)$ at $\gamma = 0.1$ as the equilibrium modulus $G(t)$. Also, all the applied strains reached the target magnitudes at $t < 0.1$ s. The step strain rise time is faster

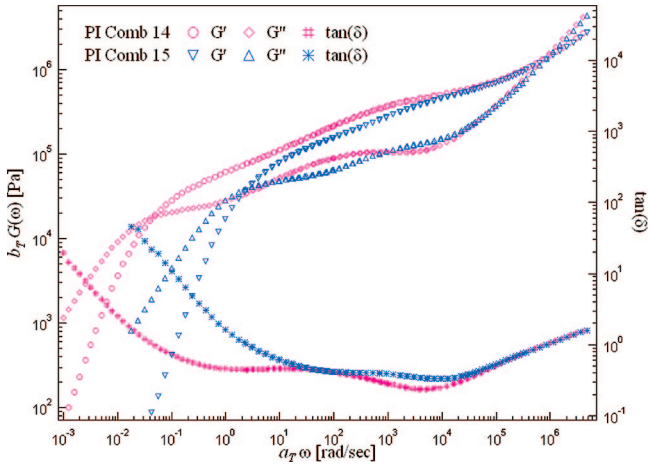

Figure 1. Experimental storage and loss moduli as well as tan(δ) of PI Comb14 and PI Comb15 at $T_{ref} = 28$ °C.

than any relaxation time except the branch relaxation time of Comb15.

3. Results and Discussion

3.1. Linear Rheology. The dynamic storage and loss moduli, $G'(\omega)$ and $G''(\omega)$, of two PI combs are shown in Figure 1. The first minimum and a hint of the second minimum appear in $G''(\omega)$, indicating the expected relaxation hierarchy of comb topology. Also, two tan(δ) minima of PI Comb14 and a hint of the second tan(δ) minimum of PI Comb15 clearly indicate the branching effect due to the entangled branches. The value of the rubbery plateau modulus G_N was evaluated as 0.45 ± 0.02 MPa by averaging $G'(\omega)$ where the first tan(δ) minimum appeared. The resulting entanglement molecular weight $M_e = (4/5)\rho RT/G_N$ of polyisoprene ($\rho = 0.9$ g/cm^3) was 4006 g/mol. The entanglement densities of each branch of PI Comb15 and PI Comb14 were around 2 and 4, respectively. The depth between the rubbery plateau region and the first $G''(\omega)$ minimum at high frequency reflected the relative branch size in these combs. It was apparent that branches with just two entanglements length sufficiently trigger the first level of the relaxation hierarchy.

In order to examine the main structural feature of comb topology, the multiple branch points along the backbone, the measured linear viscoelastic properties were compared with the predictions of the already existing hierarchy theories with the comb end effect.[6–8] This effect is due to the fact that the ends of the comb backbone are as free to move as the branches attached at the middle of backbone, so these comb ends and branches will both start to relax simultaneously. After the branch relaxation, the unrelaxed parts of the comb ends become a part of the backbone. Under the assumption of evenly distributed branch points, the molecular weight of one comb end M_{end} can be evaluated as $M_{end} = M_{bb}/(q + 1)$, with the apparent backbone molecular weight $M_{bb} = M_{total} - qM_{branch}$ and the number of branches q. If $M_{end} > M_{branch}$, the unrelaxed parts of the comb end $M_{end}(1 - s^*)$ become a part of the effective backbone as $M_{bb,eff} = (q - 1)M_{bb}/(q + 1) + 2M_{end}(1 - s^*)$. Here, the fractional distance s^* at the completion of the branch relaxation is determined by $\tau_{branch}(1) = \tau_{end}(s^*)$.

Two hierarchy theories, model I by Inkson et al.[7] and model II by Kapnistos et al.[8] without any polydispersity correction, were chosen to examine the effect on relaxation dynamics of the comb ends, which were quantified by the number of branch points. Both approaches follow the same physical picture describing the relaxation dynamics as the terminal backbone reptative motions after the backbone fluctuations following the branch relaxation. However, different values of the dilution exponent α and the numerical factors were used. The mathematical equations of model I in ref 7 were derived based on the assumption that the backbone fluctuations are governed by the drag friction from the entire backbone with $a^2 = (4/5)N_e b^2$ and $\alpha = 4/3$, while those of model II in ref 8 came from the drag friction of the half-backbone with $a^2 = N_e b^2$ and $\alpha = 1$. Here a is the original tube diameter, b is the (Kuhn) monomer length, and N_e is the number of monomers in an entanglement strand. The motion of a branch point was represented with the branch-point diffusivity $D_{bp} = p^2 a_{eff}^2/[2\tau_{branch}(1)]$, where $a_{eff} = a\phi_{bb,eff}^{-\alpha/2}$ is the effective diluted tube diameter and $p^2 = 1/12$ is the unknown hopping barrier. The early fluctuation time of the comb backbone, by analogy to a free Rouse chain, was expressed as $\tau_{bb,early}(s) = (sL_{bb,eff}/2)^2/(2D_{bb,eff})$ with the effective contour length of the backbone $L_{bb,eff} = N_{bb,eff} b^2 \phi_{bb,eff}^{\alpha/2}/a$ and the effective backbone diffusivity $D_{bb,eff} = D_{bp}/q$ in model I and $D_{bb,eff} = D_{bp}/(q/2)$ in model II. In order to match the crossover between $G'(\omega)$ and $G''(\omega)$ at the high-frequency region and the rubbery plateau region, the values of the plateau modulus G_N and the entanglement relaxation time τ_e are fixed as $G_{Nf} = 0.6$ MPa and $\tau_{ef} = 7.4$ μs, used in the earlier studies, with $M_e = 4006$ g/mol and $q = q_{model}$.

Figure 2a,b shows the predictions of models I and II for PI Comb14 along with the measured data. The molecular weight of the comb end ($M_{end} = 25.3$ kg/mol) was larger than that of the branch ($M_{branch} = 17.9$ kg/mol), so the effective backbone with the unrelaxed parts of the comb ends governs the terminal dynamics. Even though the values of numerical factors and α are different, both models I and II with $p^2 = 1/12$ quantitatively reproduced the measured data at high frequencies, where behavior is governed by the branch relaxation. However, the predicted $G'(\omega)$ and $G''(\omega)$ at the low frequencies overestimated the backbone relaxation, deviating from the experiments. Both of the values of α (4/3 and 1) yielded slower terminal dynamics for the comb backbone, as opposed to the well-predicted $G'(\omega)$ and $G''(\omega)$ of the branches. For the branch relaxation, the effect of faster dilution ($\alpha = 4/3$) with a smaller tube unit ($a^2 = (4/5)N_e b^2$) seemed to be compensated with the effect of slower dilution ($\alpha = 1$) with a larger tube unit ($a^2 = N_e b^2$). Thus, the observed discrepancies at low frequencies could be attributed to the dynamics of backbone fluctuations.

One possible source of the deviations is that the motion of the branch points along the backbone was initially limited to a local fluctuating motion, as discussed a recent study.[25] That is, the spacing between two adjacent branch points was just above the length of one branch, so the fluctuating motions of the two friction blobs (the two branch points with one branch) likely conflicted with each other, only permitting local fluctuations in the beginning, rather than allowing coordinated motions in the direction set by the entire backbone. In the previous studies,[25,26] the unknown hopping barrier p^2 was proposed as the reciprocal of the entanglement density of the unrelaxed inner parts at the next level of hierarchy instead of the arbitrarily chosen but universal $p^2 = 1/12$ for all different branched architectures. The proposed p^2 represents the frictional resistance which each branch point moving along the backbone would experience. Thus, the local early fluctuations and the coordinated fluctuations of the comb backbone could be expressed in terms of $p^2 = 1$ and $p^2 = N_e/N_{bb,eff}$, respectively. The predictions with this consideration showed reasonable agreement with the experiments in Figure 2a,b.

In the case of PI Comb15, the molecular weight of the comb end was $M_{end} = 18.1$ kg/mol, which was larger than that of branch $M_{branch} = 9.2$ kg/mol, implying that both comb ends and branches will relax simultaneously in the beginning. The

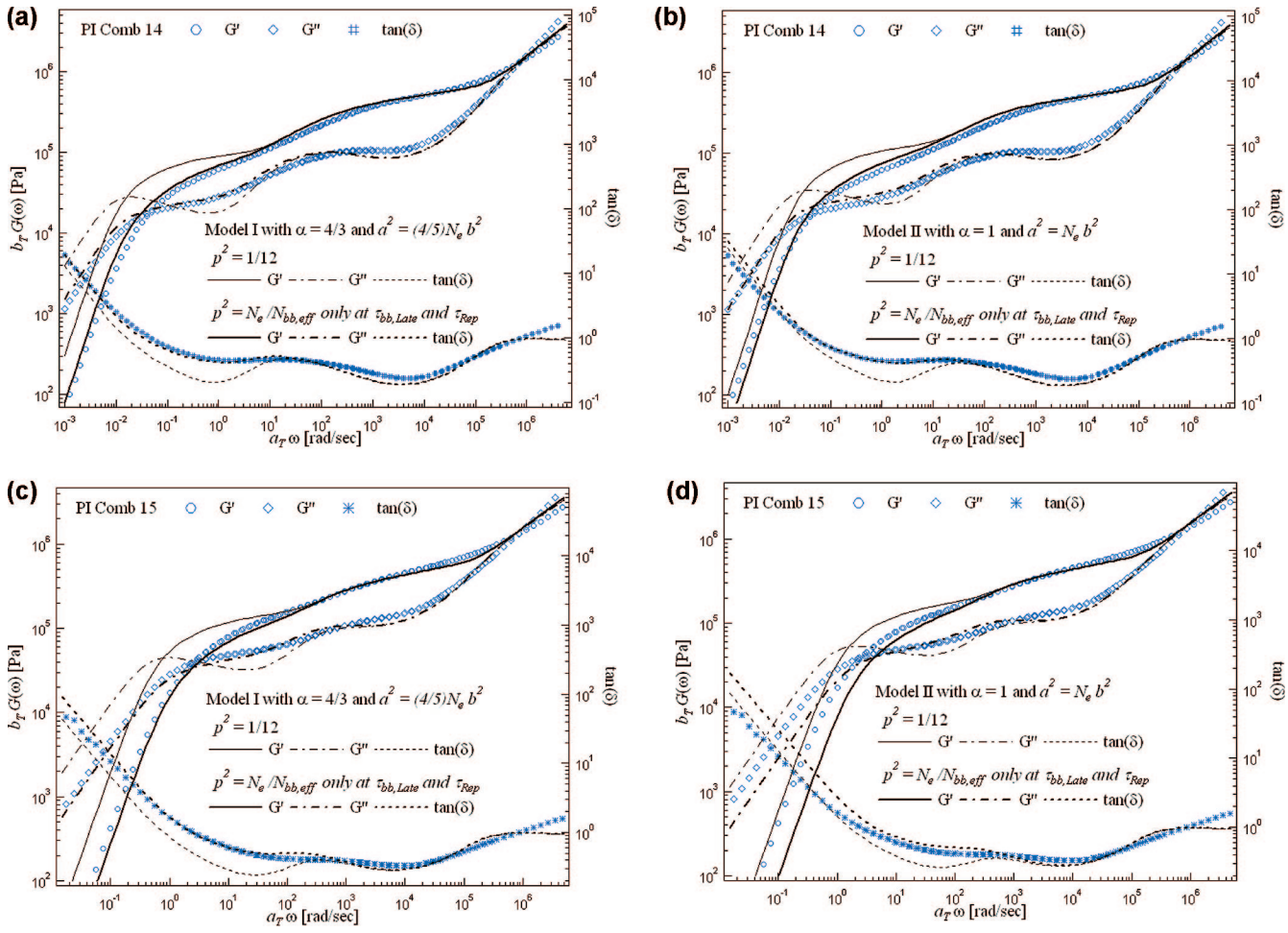

Figure 2. (a) Comparison of experimental and theoretical viscoelastic properties of PI Comb14. Lines are the predictions of model I with different values of p^2 parameter. (b) Comparison of experimental and theoretical viscoelastic properties of PI Comb14. Lines are the predictions of model II with different values of p^2 parameter. (c) Comparison of experimental and theoretical viscoelastic properties of PI Comb15. Lines are the predictions of model I with different values of p^2 parameter. (d) Comparison of experimental and theoretical viscoelastic properties of PI Comb15. Lines are the predictions of model II with different values of p^2 parameter.

predictions of the same model framework were compared with the experiments (Figure 2c,d). Again, the predicted $G'(\omega)$ and $G''(\omega)$ with the local early fluctuations reproduced the measured data better than those with randomly chosen $p^2 = 1/12$.

These simple comparisons indirectly demonstrate the presence of multiple branch points through the effects of both the comb ends and the spacing between the adjacent two branch points on the linear viscoelasticity. This can be seen even though M_{end} and $M_{spacing}$ were estimated as average values under the assumption of evenly distributed branch points along the comb backbone. It is likely that implicit structural factors like the comb ends and the spacing between the nearest two branch points would affect the relaxation dynamics of comb architectures in more complicated ways. Further theoretical studies considering the detailed distributions of branch number, the effect of unevenly arranged branches, and the resulting structural heterogeneity are still needed to complete the hierarchical theories for comb polymers, but this is not the focus of the current study.

3.2. Nonlinear Relaxation Modulus after Step Strains. The nonlinear relaxation moduli, $G(t,\gamma)$, of PI Comb14 measured after the imposition of step stains are provided in Figure 3a. At low strains, the relaxation moduli overlap at all times as a characteristic behavior of the linear deformation regime, while $G(t,\gamma)$ began to decrease with increasing the magnitude of strain, implying that the polymer was in the nonlinear deformation regime. Also, the relaxation moduli at long times became nearly parallel each other regardless of applied strains. This implies that time-strain factorability holds, meaning that $G(t,\gamma) = G(t)h(\gamma)$ for polymers with a comb topology via shifting $G(t,\gamma)$ vertically by an amount of $h(\gamma)$. Indeed, the overlap of $G(t,\gamma)h(\gamma)^{-1}$ irrespective of the applied strain was evident at times greater than ~30 s, as shown in Figure 3b. The characteristic separability time was intermediate between the evaluated terminal relaxation times, $\tau_{cross} = 1/\omega_{crossover} = 21.4$ s and $\tau_{\eta''} = 1/\omega_{\eta''} = 39.8$ s. While weak deviations were observed at very long times, at least 10 times of $\tau_{\eta''}$, these deviations are likely a result of instrumental issues with the torque signal, which becomes unreliable as it approaches its lower limit. Figure 3c provides the corresponding damping function $h(\gamma,t)$ of PI Comb14 at various discrete times. Here h_{DE} and $h_{DE\text{-}IA}$ are the predictions of the Doi−Edwards damping theory without and with the independent alignment assumption, respectively. The damping behavior of PI Comb14 clearly exhibited less strain softening (type B) than h_{DE} and $h_{DE\text{-}IA}$ at all strains. The deviation from the universal Doi−Edwards damping qualitatively reflects the degree of the backbone stretching. However, $h(\gamma,t)$ at all strains approached the Doi−Edwards predictions as time gradually increased.

It is obvious that the damping behavior of PI Comb14 was different from that of H-shaped/multibranch[3,5,18] or second-generation dendritic star[20] polymers exhibiting the branch-point withdrawal motion. The withdrawal motion appears as a novel

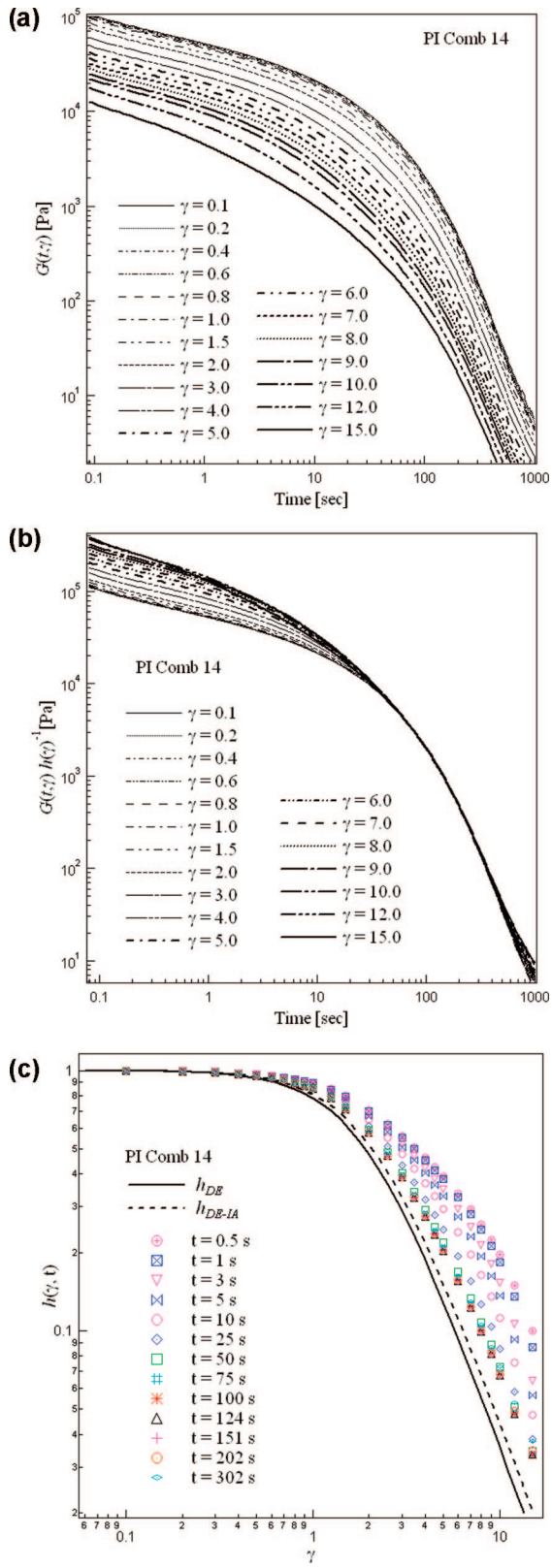

Figure 3. (a) Nonlinear shear relaxation moduli $G(t,\gamma)$ of PI Comb14 after the imposition of step strains γ. (b) Shifted nonlinear shear relaxation moduli $G(t,\gamma)h(\gamma)^{-1}$ of PI Comb14. (c) Step shear damping function $h(\gamma,t)$ of PI Comb14 at various times after the imposition of step strains γ. Lines are the predictions of the Doi−Edwards damping theory without and with the independent alignment assumption, h_{DE} and $h_{DE\text{-}IA}$, respectively.

transition in damping behavior, especially at short times, from type B to h_{DE} beyond a certain strain. Such a damping transition is a result of the immediate retraction of stretched inner parts of Y-shaped structural units in H-shaped/multibranch and second-generation dendritic star architectures. Similar to H-shaped topology, comb architecture also has comparable Y-shaped units. That is, one end of the comb backbone and one branch placed near the comb backbone end, together with the comb backbone, form a Y-shaped substructure. Under the assumption of evenly distributed branch points, the comb backbone end (M_{end} = 25.3 kg/mol), like the branch (M_{branch} = 17.9 kg/mol), is expected to exert an outward thermal tension, which comes from the arbitrary motion of the chain free end just outside of its confining tube, against the inward tension generated by the stretched backbone. Intuitively, one might expect a damping transition in $h(\gamma,t)$ of PI Comb14 due to the presence of these Y-shaped structural units. However, the measured damping behavior of PI Comb14 did not exhibit any hint of such a damping transition at any time. Rather, the deviation from the universal Doi−Edwards damping gradually decreased as time increased, which implies that the degree of the backbone stretching gradually decreased. Therefore, the observed gradual retraction according to time is a nonlinear characteristic of comb topology under the step deformations.

Also, it should be noted that the damping functions of Comb14 at long times only approached the Doi−Edwards predictions, but not reached h_{DE} and/or $h_{DE\text{-}IA}$, which was usually observed in commercial polyolefins with long-chain branches.[16,27] This behavior is quite different from the long-time damping behavior of H-shaped/multibranch or second-generation dendritic star polymers as well as linear polymers. If the branch-point withdrawal motion indeed occurs in H-shaped/multibranch or second-generation dendritic star polymers, the damping mechanism for such branched polymers becomes similar to that for linear polymers. That is, the effect of branches, which were already drawn into the confining, disappears as if there are no branches like linear polymers. On the other hand, if the branching effect from multiple branch points or generations still survives under large strains, the damping behavior might not follow the same damping picture. Since measured damping functions of well-defined but highly branched architectures are quite rare, it would be premature to specify any physical picture for the observed long-time behavior.

For the case of the comb polymer with branches of two entanglement lengths, the corresponding $G(t,\gamma)$, $G(t,\gamma)h(\gamma)^{-1}$, and $h(\gamma)$ are summarized in Figure 4. The relaxation moduli of PI Comb15 showed the general characteristics of the linear and nonlinear deformation regimes as overlapped $G(t,\gamma)$ at low strains and decreasing $G(t,\gamma)$ with increasing the magnitude of applied strains, respectively (see Figure 4a). Shifting $G(t,\gamma)$ along the y-axis yielded almost overlapping $G(t,\gamma)h(\gamma)^{-1}$ at long times beyond a time of ~0.6 s, which was comparable with the evaluated relaxation times ($\tau_{cross} = 1/\omega_{crossover} = 0.39$ s and $\tau_{\eta''} = 1/\omega_{\eta''} = 0.75$ s). Considering these relaxation times, the inexact overlapping at very long time again likely reflects mechanical limits, rather than material properties. The corresponding $h(\gamma,t)$ at discrete times shown in Figure 4c exhibited much weaker type B behavior than those of PI Comb14, probably due to the shorter length of the branches, but still appeared above h_{DE} and $h_{DE\text{-}IA}$. Although the deviation from the universal Doi−Edwards damping is not so large as the deviation observed in PI Comb14, $h(\gamma,t)$ of PI Comb15 at all strains fell toward h_{DE} and $h_{DE\text{-}IA}$ with increasing the observation time. This is consistent with the damping behavior of PI Comb14, supporting the physical picture of a gradual retraction according to time due to multiple branch points.

In order to illustrate the rheological characteristics of specific structural units, the linear viscoelasticity and damping behavior of PI Comb14 were compared with those of second-generation

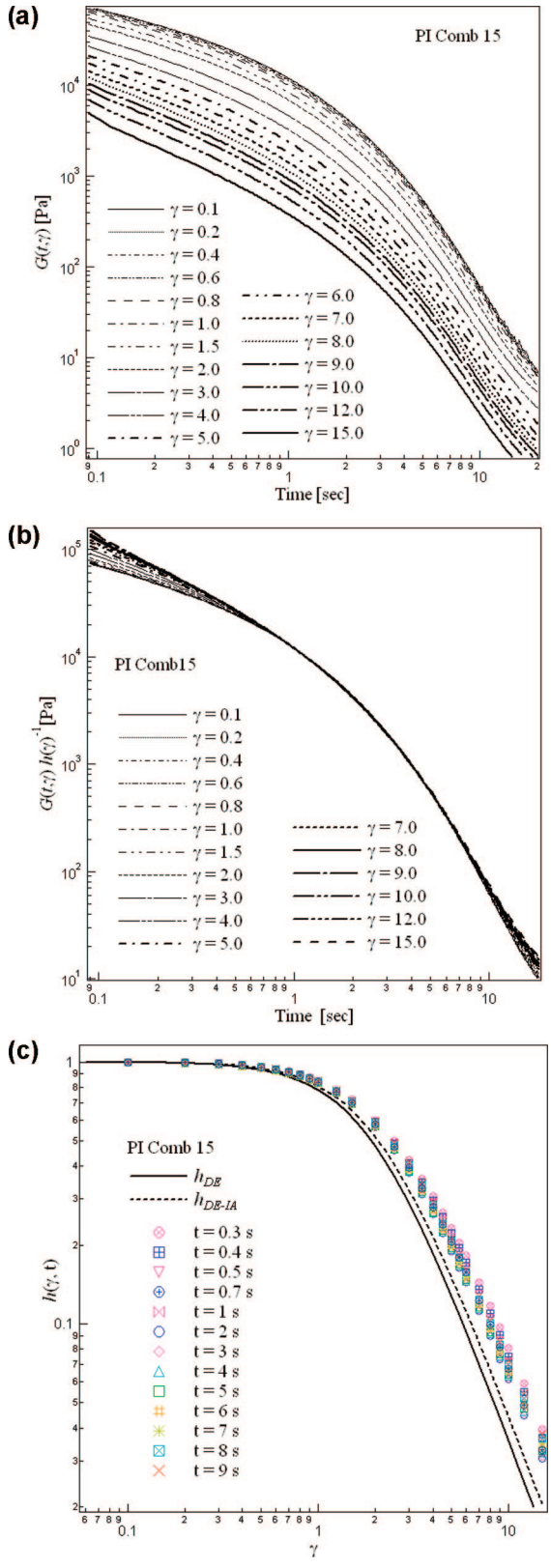

Figure 4. (a) Nonlinear shear relaxation moduli $G(t,\gamma)$ of PI Comb15 after the imposition of step strains γ. (b) Shifted nonlinear shear relaxation moduli $G(t,\gamma)h(\gamma)^{-1}$ of PI Comb15. (c) Step shear damping function $h(\gamma,t)$ of PI Comb15 at various times after the imposition of step strains γ. Lines are the predictions of the Doi−Edwards damping theory without and with the independent alignment assumption, h_{DE} and $h_{DE\text{-}IA}$, respectively.

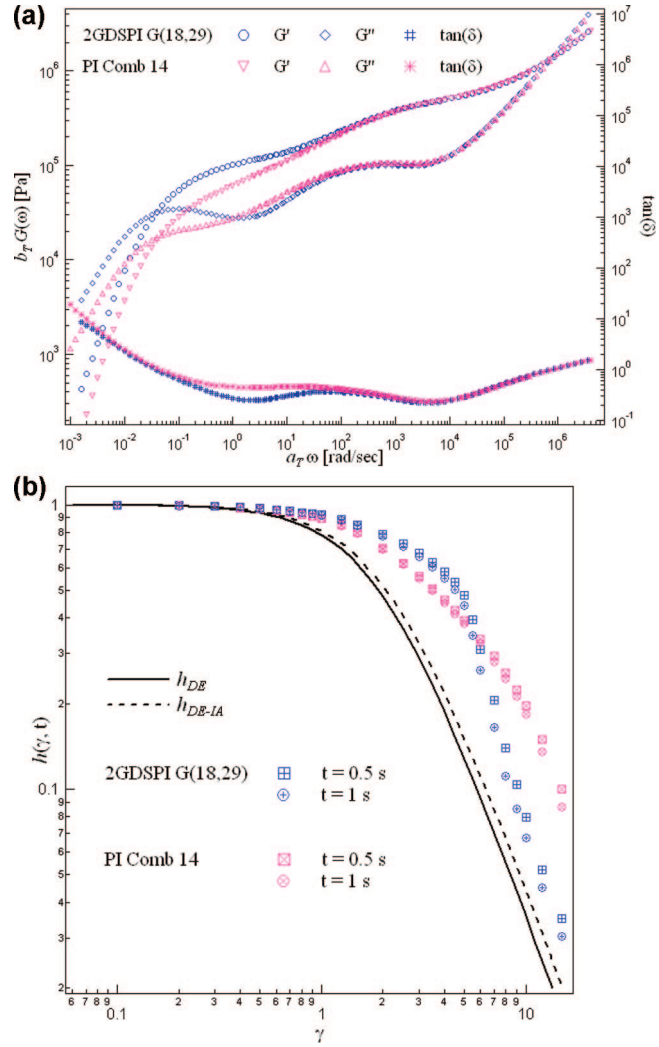

Figure 5. (a) Experimental storage and loss moduli as well as tan(δ) of the second-generation dendritic polyisoprene star polymer, 2GDSPI G(18,29), and the polyisoprene comb polymer, PI Comb14, at T_{ref} = 28 °C. (b) Step shear damping function $h(\gamma,t)$ of 2GDSPI G(18,29) and PI Comb14 at short times after the imposition of step strains γ. Lines are the predictions of the Doi−Edwards damping theory without and with the independent alignment assumption, h_{DE} and $h_{DE\text{-}IA}$, respectively.

dendritic star polyisoprene[20] 2GDSPI G(18,29). The center of this molecule is a symmetric three-branch star with the first-generation branches ($M_{w,G\text{-}1}$ = 29.7 kg/mol), the free ends of which are linked to two second-generation branches ($M_{w,G\text{-}2}$ = 18.5 kg/mol). The linear rheology data in Figure 5a clearly present two minima in tan(δ) as a signature of the expected relaxation hierarchy of two due to the faster relaxing outer branches, $M_{w,branch}$ in PI Comb14 and $M_{w,G\text{-}2}$ in 2GSPI G(18,29). The nearly exact overlap of $G'(\omega)$ and $G''(\omega)$ at high frequency for these two structurally different polymers was likely due to the fact that the outer branches of each were of similar molecular weight and so affected the relaxation dynamics similarly. However, the different magnitudes of $G'(\omega)$ and $G''(\omega)$ at low frequency reflected the differences in the nature of the slower relaxing inner parts in each topology. Interestingly, the evaluated relaxation times, $\tau_{cross} = 1/\omega_{crossover}$, are almost same as around 20 s, even though the detailed architectures were quite different. More interestingly, the second tan(δ) minimum in the both polymers appeared near ω = 2 rad/s. This implies the dilution of the entanglement network by the outer branches was completed at almost the same time. However, the degree of tube dilution in PI Comb14 seems larger than that in 2GDSPI G(18,29) when the magnitudes of the second plateau modulus

are considered. If these linear rheology data were given alone without any structural information, it would be very difficult to determine even whether these polymers had the same type of architecture or not. For example, the observed differences in linear rheology can be caused by variations in the total number of branches or the length of backbone in comb topology, rather differences in topology, like those between H-shaped/multibranch and comb polymers.

However, the corresponding damping behavior in Figure 5b clearly shows the effect of different architectures, especially at short times. The damping function of 2GDSPI G(18,29) exhibited a change in the damping behavior from type B toward the universal Doi−Edwards damping beyond a certain strain, while $h(\gamma,t)$ of PI Comb14 kept displaying less strain softening at all strains. Figure 5b with above linear rheology data provides several insights into the effect of architectures on the damping mechanism. One is that the observed damping transition does indeed come from pulling the branch point as well as two branches ($M_{w,G-2}$) into the confining tube, rather than embracing these two branches within the widened confining tube created by the already relaxed outer branches (i.e., tube dilution). As mentioned earlier, the length of the outer branches for 2GDSPI G(18,29) was nearly equal to that of those for PI Comb14, so their ability to hinder the retraction process was expected to be similar for both architectures. Moreover, the degree of dilution in PI Comb14 is more than that in 2GDSPI G(18,29), implying a wider effective tube diameter in PI Comb14 (see Figure 5a). In terms of the size of the tube, it is possible that the longitudinal stretching of the confining tube would result in a reduced tube diameter from its equilibrium value. Thus, there might be a competition between the rates of the tube diameter recovery by the retraction process and the tube dilution by the outer branch relaxation. Nonetheless, the damping transition from type B to the universal Doi−Edwards damping only occurs in $h(\gamma,t)$ of 2GDSPI G(18,29). Therefore, we can conclude that the branch-point withdrawal motion is a nonlinear characteristic of a specific architecture, arising from the sudden retraction of the Y-shaped structural units.

Another conclusion is that the presence of multiple branches seems to affect not only the retracting but also the stretching motions of the inner parts. The magnitudes of the type B behavior of PI Comb14 at the early stages of the nonlinear deformation regime were lower than those of 2GDSPI G(18,29). This implies either that the degree of the backbone stretch in the comb topology was relatively less than that in dendritic topology or that the backbone stretch relaxation of PI Comb14 is faster than that of 2GDSPI G(18,29). One can imagine that the lower magnitude of type B behavior of PI Comb14 was a result of a faster stretch relaxation (or faster retraction process). In the earlier studies of H-shaped/multibranch polymers, which consist of symmetric Y-shaped units like 2GDSPI G(18,29), the stretch relaxation time[3,19] was expressed in terms of to the length of inner backbone M_{bb}/M_e, the number of branches q, and the outer branch relaxation time $\tau_{branch}(1)$, $\tau_{stretch} \sim (M_{bb}/M_e)\tau_{branch}(1)q$. If the size of unrelaxed inner parts and the number of outer branches in comb topology are considered, the faster stretch relaxation would be more plausible in 2GDSPI G(18,29). A simplest estimate, with q as the number of branches but without any numerical prefactor and the dilution effect, yields $\tau_{stretch} \sim 2.4$ s for the symmetric Y-shaped unit of 2GDSPI G(18,29), the two outer arms with one inner arm. The stretch relaxation time for the corresponding symmetric unit of Comb14 (e.g., the half of Comb14) is $\tau_{stretch} \sim 5.4$ s, while that for the entire Comb14 is $\tau_{stretch} \sim 25.4$ s. On the other hand, it is also possible that the inner sections of 2GDSPI G(18,29) were stretched more than those of PI Comb14 because there were no branches present to hinder the stretching itself, unlike PI Comb14. In this viewpoint, the observed magnitude differences in type B behavior suggest that the multiple branches (or multiple branch points) in the middle of the backbone induce gradual stretching as well as retracting motions in comb topology.

4. Conclusion

We have studied the stress relaxation dynamics of well-defined, entangled polyisoprene comb polymers under small-amplitude oscillatory shear and nonlinear step deformations. These experimental data provide rheological characteristics that are unique to the comb topology, arising from the multiple branch points along the linearlike backbone. These characteristics are especially evident under nonlinear deformations. The observation of two tan(δ) minima, a signature of the relaxation hierarchy of two, validated the presence of the entangled branches in current comb polymers. Also, simple comparisons between the measured linear viscoelasticity and the predictions of the hierarchy theories indirectly demonstrated the existence of the multiple branch points in terms of (1) the relaxation of the comb ends and (2) the effect of the spacing between adjacent two branch points described as the dominant local early fluctuations in the backbone relaxation dynamics.

Stress relaxation behavior after the imposition of step shear deformations provided insight into the nonlinear features of the multiple branch points in comb topology. A damping function defined as the ratio of nonlinear modulus to the equilibrium modulus is a simple measure of the stretched state of chain segments. The damping behavior of entangled comb polymers clearly exhibited less strain softening (type B) than the universal Doi−Edwards damping functions (h_{DE} and $h_{DE\text{-}IA}$) at all strains. However, the corresponding damping functions gradually approach h_{DE} and $h_{DE\text{-}IA}$ as the observation time increases. The observed type B behavior, lasting at all strains but gradually approaching the universal Doi−Edwards damping according to time, was clearly different from the damping behavior of H-shaped/multibranch and dendritic star polymers, showing a novel damping transition from type B to h_{DE} as the branch-point withdrawal motion. The latter represents a sudden retraction at large strains due to the Y-shaped structural units, while the former corresponds to a gradual retraction at all strains due to the multiple branch points. Thus, the damping mechanism in comb topology is gradual stretching and retracting motions caused by the multiple branch points placed along the linearlike comb backbone. Also, rheological features in the damping behavior, the damping transition and the gradual retraction, could be useful as a means to extract information on specific structural variables, even when the details of branched architectures are not available from direct characterization.

References and Notes

(1) Doi, M.; Edwards, S. F. *The Theory of Polymer Dynamics*; Oxford University Press: New York, 1986.
(2) Milner, S. T.; McLeish, T. C. B. *Macromolecules* **1997**, *30*, 2159.
(3) McLeish, T. C. B. *Macromolecules* **1999**, *32*, 6738.
(4) Juliani; Archer, L. A. *Macromoleculesv* **2002**, *35*, 10048.
(5) Archer, L. A.; Juliani, *Macromolecules* **2004**, *37*, 1076.
(6) Daniels, D. R.; McLeish, T. C. B.; Crosby, B. J.; Young, R. N.; Fernyhough, C. M. *Macromolecules* **2001**, *34*, 7025.
(7) Inkson, N. J.; Graham, R. S.; McLeish, T. C. B.; Groves, D. J.; Fernyhough, C. M. *Macromolecules* **2006**, *39*, 4217.
(8) Kapnistos, M.; Vlassopoulos, D.; Roovers, J.; Leal, L. G. *Macromolecules* **2005**, *38*, 7852.
(9) Pantazis, D.; Chalari, I.; Hadjichristidis, N. *Macromolecules* **2003**, *36*, 3783.
(10) Vazaios, A.; Hadjichristidis, N. *J. Polym. Sci., Part A: Polym. Chem.* **2005**, *43*, 1038.
(11) Koutalas, G.; Iatrou, H.; Lohse, D. J.; Hadjichristidis, N. *Macromolecules* **2005**, *38*, 4996.

(12) Driva, P.; Iatrou, H.; Lohse, D. J.; Hadjichristidis, N. *J. Polym. Sci., Part A: Polym. Chem.* **2005**, *43*, 4070.
(13) Orfanou, K.; Iatrou, H.; Lohse, D. J.; Hadjichristidis, N. *Macromolecules* **2006**, *39*, 4361.
(14) Driva, P.; Lohse, D. J.; Hadjichristidis, N. *J. Polym. Sci., Part A: Polym. Chem.* **2008**, *46*, 1826.
(15) McLeish, T. C. B. *Macromolecules* **1988**, *21*, 1062.
(16) Osaki, K. *Rheol. Acta* **1993**, *32*, 429.
(17) Bick, D. K.; McLeish, T. C. B. *Phys. Rev. Lett.* **1996**, *76*, 2587.
(18) Archer, L. A.; Varshney, S. K. *Macromolecules* **1998**, *31*, 6348.
(19) McLeish, T. C. B.; Larson, R. G. *J. Rheol.* **1998**, *31*, 6348.
(20) Lee, J. H.; Orfanou, K.; Driva, P.; Iatrou, H.; Hadjichristidis, N.; Lohse, D. J. *Macromolecules* **2008**, *41*, 9165.
(21) Vega, D. A.; Milner, S. T. *J. Polym. Sci., Part B: Polym. Phys.* **2007**, *45*, 3117.
(22) Frischknecht, A. L.; Milner, S. T.; Pryke, A.; Young, R. N.; Hawkins, R.; McLeish, T. C. B. *Macromolecules* **2002**, *35*, 4801.
(23) Gotro, J. T.; Graessley, W. W. *Macromolecules* **1984**, *17*, 2767.
(24) Abdel-Goad, M.; Pyckhout-Hintzen, W.; Kahle, S.; Allgaier, J.; Richter, D.; Fetter, L. J. *Macromolecules* **2004**, *37*, 8135.
(25) Lee, J. H.; Fetters, L. J.; Archer, L. A. *Macromolecules* **2005**, *38*, 10763.
(26) Lee, J. H.; Fetters, L. J.; Archer, L. A. *Macromolecules* **2005**, *38*, 4484.
(27) Stadler, F. J.; Auhl, D.; Münstedt, H. *Macromolecules* **2008**, *41*, 3720.

MA8022662